



Fluorescence Correlation Spectroscopy with Photobleaching Correction in Slowly Diffusing Systems

Cameron Hodges¹ · Rudra P. Kafle^{1,2} · J. Damon Hoff¹ · Jens-Christian Meiners^{1,3}

Received: 9 August 2017 / Accepted: 15 January 2018
© Springer Science+Business Media, LLC, part of Springer Nature 2018

Abstract

Fluorescence correlation spectroscopy (FCS) is a powerful tool to quantitatively study the diffusion of fluorescently labeled molecules. It allows in principle important questions of macromolecular transport and supramolecular aggregation in living cells to be addressed. However, the crowded environment inside the cells slows diffusion and limits the reservoir of labeled molecules, causing artifacts that arise especially from photobleaching and limit the utility of FCS in these applications. We present a method to compute the time correlation function from weighted photon arrival times, which compensates computationally during the data analysis for the effect of photobleaching. We demonstrate the performance of this method using numerical simulations and experimental data from model solutions. Using this technique, we obtain correlation functions in which the effect of photobleaching has been removed and in turn recover quantitatively accurate mean-square displacements of the fluorophores, especially when deviations from an ideal Gaussian excitation volume are accounted for by using a reference calibration correlation function. This allows quantitative FCS studies of transport processes in challenging environments with substantial photobleaching like in living cells in the future.

Keywords Fluorescence correlation spectroscopy · Live-cell microscopy · Photobleaching · Cellular transport · Sub-diffusion

Introduction

Fluorescence correlation spectroscopy (FCS) has, since its introduction in 1972, become a powerful tool to quantitatively study the diffusion of fluorescent molecules [1]. It owes its popularity in no small part to the fact that it is non-invasive and can be carried out on a standard confocal microscope, and is compatible with automated microscopy systems that are a staple of biomedical and pharmaceutical research.

The principle behind FCS is simple: As the molecules diffuse in and out of a small volume illuminated by a laser,

the fluorescence intensity $I(t)$ is recorded. From these traces, time correlation functions

$$G(\tau) = \langle I(t) \cdot I(t + \tau) \rangle_t \quad (1)$$

are computed. For simple diffusion of a single species of molecules, the time autocorrelation of the fluorescence intensity has the functional form [2]

$$G(\tau) = G(0) \left(1 + \frac{\tau}{\tau_D}\right)^{-1} \left(1 + \frac{\tau}{A^2 \tau_D}\right)^{-1/2} \quad (2)$$

where $A = \omega_z / \omega_{xy}$ is the aspect ratio of the excitation volume, given by the radial and axial half-widths ω_{xy} and ω_z of the excitation volume. τ_D is the average residence time of the molecules in the excitation volume. Fitting the experimentally obtained autocorrelation function to Eq. (2) allows then the extraction of the diffusion coefficient $D = \omega_{xy}^2 / 4\tau_D$.

Traditionally FCS studies are carried out in aqueous solution, where diffusion is fast and a large reservoir of sample molecules is present. This typically minimizes adverse effects from photobleaching, as each fluorophore is illuminated only very briefly, and, if it is bleached, rapidly

✉ Jens-Christian Meiners
meiners@umich.edu

¹ Department of Biophysics, University of Michigan, 930 N. University Ave., Ann Arbor, MI 4809-1055, USA
² Department of Physics, Worcester Polytechnic Institute, 100 Institute Rd., Worcester, MA 01609-2280, USA
³ Department of Physics, University of Michigan, 450 Church St., Ann Arbor, MI 48109-1120, USA

replaced. With the growing accessibility and popularity of FCS, however, FCS is increasingly being used in systems where diffusion is slow or confined, like in living cells or complex fluids. Examples include inquiries into membrane structure and dynamics [3], intracellular protein diffusion [4–6], transcription factor binding to nuclear DNA [7], and the molecular basis for cell–cell interactions [8]. In these systems, diffusion is often slow, constrained, and perhaps sub-diffusive. Now the destruction of fluorophores through photobleaching becomes a significant concern, as a significant fraction of the bleached molecules is no longer replenished [9]. As a consequence, additional time constants are introduced into the dynamics of the system. While this feature has been exploited to study the photobleaching process itself [10], it is generally problematic because it distorts the autocorrelation functions and makes conventional quantitative analysis fraught with errors, if not impossible.

In this article we present a method to compute the autocorrelation function in a way that numerically compensates for the effects of photobleaching as part of the data analysis procedure. This method is based on constructing the autocorrelation function from pairs of arrival times of the photons, which are recorded during the measurement in a time-tagged mode, using an adaptation of the algorithm of Wahl et al. [11]. To account for photobleaching, we assign each photon pair in the computation a different weight that is determined by the arrival times, with late arriving photons being weighted more heavily than earlier ones. This compensates for the loss of fluorophores to photobleaching. We test and validate this method with FCS photon arrival time data obtained from numerical simulations and fluorophores diffusing in glycerol solutions, and demonstrate that the thus obtained correlation functions are essentially identical to those that would have been obtained if the fluorophores were perfectly photostable.

We further use these corrected correlation functions to extract the mean-square displacement of the particles. We compare the customary method that relies on an analytical relationship between mean-square displacement and correlation function for a Gaussian excitation volume with an empirical calibration that makes no assumption about the beam shape and obtain generally superior results especially for long time and length scales.

Computational

The starting point for the generation of simulated FCS photon arrival times is the computation of three-dimensional random walks for particles that cross the excitation volume of a laser beam. For this aim, we used the stochastic differential equation simulator in the Financial Toolbox of MATLAB to simulate the trajectories of 100 particles over

60 s with 1 μ s time steps, using 12 CPU cores on a shared high-performance cluster computer. The pertinent equation of motion describing the Wiener process for the particle position X is

$$dX = \sqrt{(2k_B T / \zeta)} dt dW \quad (3)$$

where ζ is the friction coefficient of the particle and dW a white-noise Brownian force acting on the particle. In our simulations, the friction coefficients ranged from $\zeta = 10^{-11}$ kg s $^{-1}$ to $\zeta = 10^{-8}$ kg s $^{-1}$, which corresponds to diffusion coefficients spanning the range from small molecules in water to the diffusion of genetic loci in *E. coli* [12], and membrane proteins in between [13].

Periodic boundary conditions were applied to these trajectories to confine the particles to a 2 μ m \times 2 μ m \times 2 μ m box to maintain a constant particle concentration in the simulation volume. The probability of exciting and detecting a photon from a fluorophore i located at (x, y, z) is then modeled by a three-dimensional Gaussian probability distribution with the radial and axial half-widths $\omega_{xy} = 250$ nm and $\omega_z = 1250$ nm,

$$p_i(x, y, z) = e^{-(x+y)^2 / \omega_{xy}^2 - z^2 / \omega_z^2} \quad (4)$$

as shown in Fig. 1. Photon arrival times can then be generated by using a random number generator with a combined probability distribution $p(t) = \sum_i p(x_i(t), y_i(t), z_i(t))$ for all particles.

Photobleaching is implemented in this model by dividing the particles into three distinct populations: those with a fast photobleaching rate k_{fast} , those that bleach more slowly with a rate k_{slow} , and those that are persistent and do not photobleach at all. For each particle in the first two groups we then assign a random cutoff time c_i at which photobleaching occurs, using an exponential lifetime distribution $p_{PB}(t) = ae^{-kt}$ with the appropriate fast or slow decay constant k . The probability of detecting a photon at time t is then

$$p(t) = \sum_{i \text{ fast}} p_i(t) H(t - c_i) + \sum_{i \text{ slow}} p_i(t) H(t - c_i) + \sum_{i \text{ persistent}} p_i(t) \quad (5)$$

where H is the Heaviside step function. This results in a double-exponential decay of the number of fluorescent particles and hence the average intensity

$$\hat{I}(t) = a_{fast} e^{-k_{fast} t} + a_{slow} e^{-k_{slow} t} + y_0 \quad (6)$$

in the simulation volume. Empirically the use of this double-exponential decay with a baseline, or three populations of fluorophores, describes photobleaching in our experimental samples quite well. We then use the photon detection probability in Eq. (5) to randomly generate photon arrival times as they would be seen on a detector in an actual experiment.

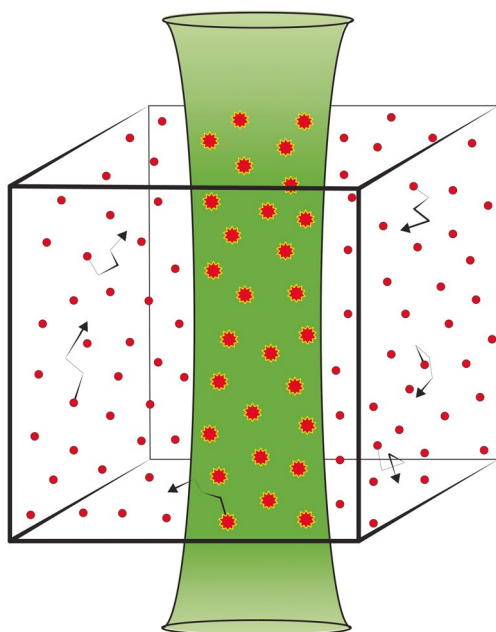


Fig. 1 Simulation of FCS data. The trajectories of 100 freely diffusing particles inside a box of $2\ \mu\text{m} \times 2\ \mu\text{m} \times 2\ \mu\text{m}$ with periodic boundary conditions are computed. From these trajectories, the fluorescence intensity for excitation and detection in a Gaussian confocal volume of $250\ \text{nm} \times 250\ \text{nm} \times 1250\ \text{nm}$ is calculated. This intensity curve yields a probability distribution that represents photon excitation, emission, and detection probability, which in turn is used to generate simulated photon arrival time data

For most of the simulations the average photon rate was set to 10^6 photons per second for all particles combined and before photobleaching.

Experimental

FCS data on dye solutions in glycerol as slowly diffusing model systems were collected using an ISS ALBA time-resolved confocal microscope, with an IX-81 Olympus microscope body and a U-Plan S-APO 60X water immersion objective (1.2 NA, 0.28 mm working distance). A Fianium supercontinuum laser with an acousto-optical filter was used to generate picosecond-excitation pulses at a wavelength of 630 nm at a repetition rate of 20 MHz. The laser power was varied to induce different amounts of photobleaching in the sample. Typically, we used 82.5 μW , 48.5 μW , or 14.3 μW of laser power entering the back aperture of the objective. Fluorescence was collected through a 50 μm pinhole and a $700 \pm 32\ \text{nm}$ bandpass filter onto a low noise avalanche photodiode. Arrival times were recorded in time-tagged mode for each photon.

Cy5 samples consisted of 10 μL 50 nM Cy5 dye (Thermo Fisher Scientific) solution in 90 μL of glycerol, or for comparison TBE buffer (pH 8.0). At room temperature,

the glycerol solution has a dynamic viscosity [14] of $\eta = 0.21\ \text{N s/m}^2$, which is about 200x the viscosity of an aqueous solution and not unlike the viscosity encountered inside living cells. Laser-induced viscosity changes due to heating of the sample volume by absorption of the excitation light were deemed negligible, as the dye solution has an absorption coefficient of at most $10\ \text{m}^{-1}$, which corresponds to a heating coefficient of 10 K/W of incident laser light [15].

Data acquisition and calibrations were done using VistaVision software. Beam parameters for the excitation volume were determined by taking FCS data for Cy5 in TBE buffer at 50 nM, 5 nM, 0.5 nM, and 50 pM concentrations. The VistaVision software package allows a global simultaneous least-square fit to these curves, which in turn yields the beam parameters.

Data Analysis

Photobleaching Correction

The input for the photobleaching correction algorithm are the arrival times t_i of every photon, as recorded by the FCS detector in time-tagged mode, or generated numerically in our simulations. The starting point for the photobleaching correction is to determine the overall extent of the photobleaching in our data. For this aim, the photon arrival data is binned into a histogram that provides the intensity as a function of time $I(t)$, which is then fitted to the double-exponential decay of Eq. (6), which in turn yields the amplitudes and time constants of the observed photobleaching. The intensity autocorrelation function, however, is not calculated from this curve, but directly from the photon arrival times using a method based on an algorithm by Wahl et al. [11]. In this scheme the autocorrelation function is calculated as the number of all pairs of photons falling into a particular lag time interval τ_k . As the algorithm progresses to larger lag time intervals, time-scale coarsening is implemented by combining multiple photons into one entry and giving them a weight w_i that corresponds to the number of combined photons. This algorithm forms the basis for our correction method: To account for photobleaching we modify this scheme to assign each photon a starting weight $w_i = I^{-1}(t_i)$, instead of one, to compensate for missing photons from fluorophores that have already been lost to photobleaching. Time-scale coarsening proceeds as usual by adding the weights of all combined photons. With this modification, we obtain time correlation functions that reflect only the dynamics of the molecules themselves and no longer show the additional correlations that are introduced by photobleaching.

Mean-Square Displacement Reconstruction

From the photobleaching-corrected autocorrelation function we then calculate the mean-square displacement $\langle \Delta r^2(\tau) \rangle$ of the fluorophores. Generally, the normalized FCS autocorrelation function is related to the mean-square displacement by

$$G(\tau) = G(0) \left(1 + \frac{2\langle \Delta r^2(\tau) \rangle}{3\omega_{xy}^2} \right)^{-1} \left(1 + \frac{2\langle \Delta r^2(\tau) \rangle}{3\omega_z^2} \right)^{-1/2} \quad (7)$$

where ω_{xy} and ω_z are the radial and axial half-widths of the Gaussian excitation volume. This, however, holds strictly only for normal diffusion. Kubečka et al. [16] have shown through simulations, though, that even in the case of labeled segments on a polymer in solution where diffusion is anomalous over a wide range of time scales Eq. (7) is a very good approximation. For the present study, we are therefore using a numerical inversion of Eq. (7) generated from a look-up-table to calculate mean-square displacements from the normalized correlation functions.

A problem that we encounter with using Eq. (7) is that it assumes a perfect Gaussian beam profile. Deviations from the ideal beam shape will result in errors at long time scales when diffusing particles reach outlying areas of the excitation volume. To account for this, we also implemented a scheme in which the mean-square displacement of the particles of interest is calculated from a calibration data set $G_{cal}(\tau)$ with dye molecules of known diffusion coefficient D_{cal} . The mean-square displacement of a particle can then be calculated from the measured correlation function $G(\tau)$ and a numerical inversion of the calibration function $G_{cal}^{-1}(\tau)$:

$$\langle \Delta r^2(\tau) \rangle = 6D_{cal} G_{cal}^{-1}(G(\tau)). \quad (8)$$

Equation (8) no longer makes any assumptions about the shape of the excitation volume and can be used when there are significant distortions at longer time and length scales.

Results and Discussion

Three-dimensional trajectories for 100 particles diffusing freely inside a $2 \mu\text{m} \times 2 \mu\text{m} \times 2 \mu\text{m}$ box with a friction coefficient of $\zeta = 10^{-8} \text{ kg s}^{-1}$, corresponding to a diffusion coefficient of $4 \cdot 10^{-13} \text{ m}^2 \text{ s}^{-1}$ were computationally generated. These trajectories were used to generate three sets of photon arrival times: the first for $6 \cdot 10^7$ photons without photobleaching, the other two with random truncations of the photon streams from the particles to simulate various degrees of photobleaching. For weak photobleaching, bleaching rates of 0.33 and 0.033 s^{-1} were assumed for a population of particles where 25% bleach rapidly, 25%

slowly, and the remaining half persist without ever bleaching. For strong photobleaching we used the same rates, but population ratios of 45, 45, and 10%, respectively. Binning the photon arrival times yields the intensity as a function of time, as shown in Fig. 2a, together with double-exponential fits as per Eq. (6).

From the photon arrival times we used our algorithm as described above to directly compute the time autocorrelation functions for all three data sets. As shown in Fig. 2b, photobleaching induces long time correlations into the data, making further quantitative analysis, such as attempts to determine diffusion coefficients from these raw correlation functions, difficult if not impossible. To obtain correlation functions that are untainted by the effects of photobleaching, we use our weighting algorithm described above to account

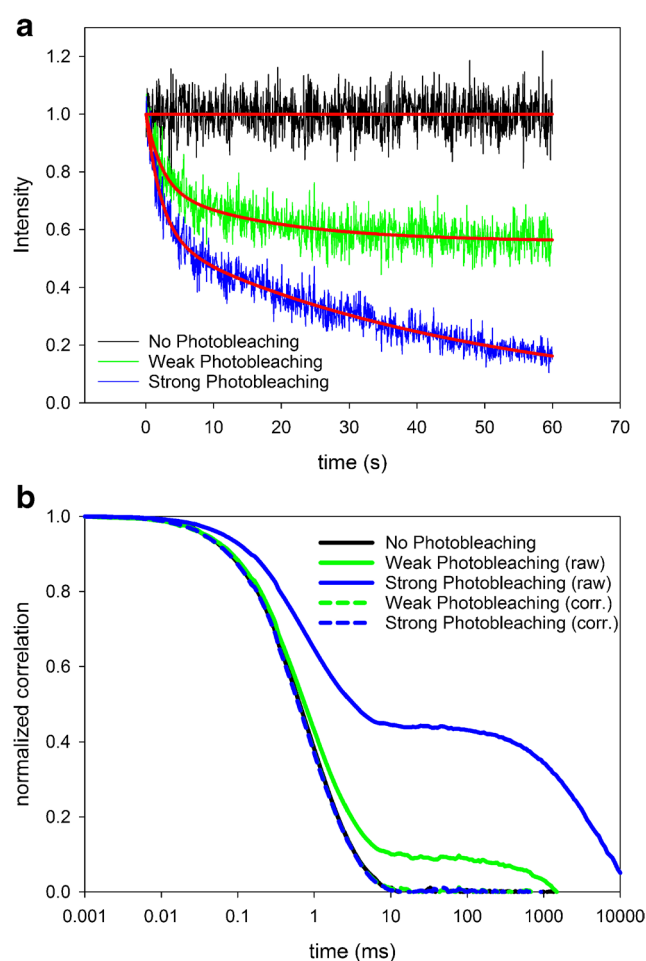


Fig. 2 Correcting FCS autocorrelation functions for photobleaching. **a** shows the fluorescence intensity as a function of time, together with bi-exponential fits, as computed from simulated photon arrival times with strong (blue), weak (green) and no photobleaching (black). **b** shows the time correlation functions that are computed from these photon arrival times with and without the photobleaching correction. After applying our correction algorithm, all curves are indistinguishable from the curve in the absence of photobleaching

for the loss of fluorophores during the observation time. The weight of each photon was determined from the parameters of the double-exponential fits. The resultant corrected correlation functions now fall virtually indistinguishably on the correlation function without photobleaching. This demonstrates the power of our algorithm to almost completely remove artifacts related to photobleaching from the correlation functions.

We then explored how well we can recover mean-square displacements from the correlation functions using a lookup-table based numerical inversion of Eq. (7). For comparison, we also calculated the mean-square particle displacement directly from the particle trajectories. The results are shown in Fig. 3. For the larger particles with a friction coefficient $\zeta = 10^{-8} \text{ kg s}^{-1}$ we recover their root-mean square displacement with an accuracy of 15% for a range of absolute displacements from 15 to 750 nm. For the smaller particles with $\zeta = 10^{-10} \text{ kg s}^{-1}$, the accuracy is somewhat reduced: we recover the root-mean square displacement with an accuracy of about 35% for a range of 35 nm to 1 μm . We notice especially that the recovered mean-square displacement is reduced for short time scales for the small particles, which artificially gives the impression of slightly superdiffusive behavior with an exponent of $\nu = 1.19$, even though the particles diffuse normally in the simulations.

To demonstrate the utility of our approach in an actual experimental system, we looked at the diffusion of Cy5 dye molecules in glycerol solution. The increased viscosity of the glycerol solution slows the dye diffusion about 200-fold compared to aqueous solution and, as a result, increases the residence time of the molecules in the excitation volume of the laser to the point where photobleaching becomes a

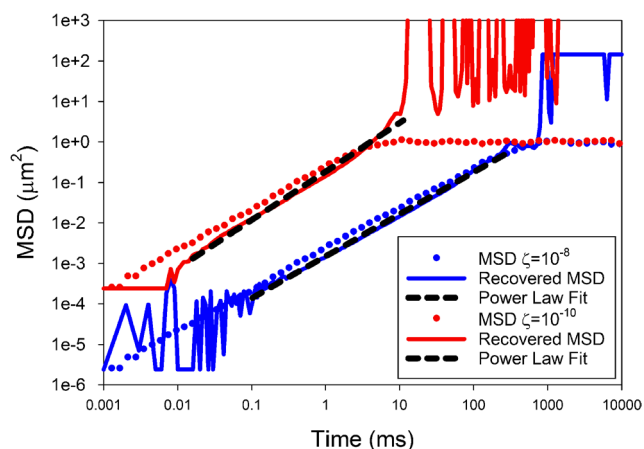


Fig. 3 Mean-square displacement of the particles for two different friction coefficients. The dotted lines show the displacements as calculated directly from the particle trajectories, and the solid lines the mean-square displacements that are recovered from the correlation functions of the photon streams through numerical inversion of Eq. (7). Fits to power laws are indicated as dashed lines

noticeable problem. This mimics the situation inside a cell, where diffusion is generally constrained and slowed by the surrounding crowded environment. Unlike in the simulations, we are unable to turn photobleaching off in the real experimental system. We can, however, reduce the intensity of the excitation laser substantially to reduce its effect; this comes, however, at the price of a reduced signal, making the data overall noisier.

Figure 4 shows the data for different excitation intensities. For 82.5 μW of laser power going into the objective, photobleaching is quite pronounced, whereas it is almost non-existent at 14.3 μW . When we calculate autocorrelation functions from the raw, uncorrected data, the curves depend very significantly on the excitation intensity. This effect is solely attributable to photophysical processes like photobleaching, as the underlying diffusive motion does not change. When we employ our correction algorithm and

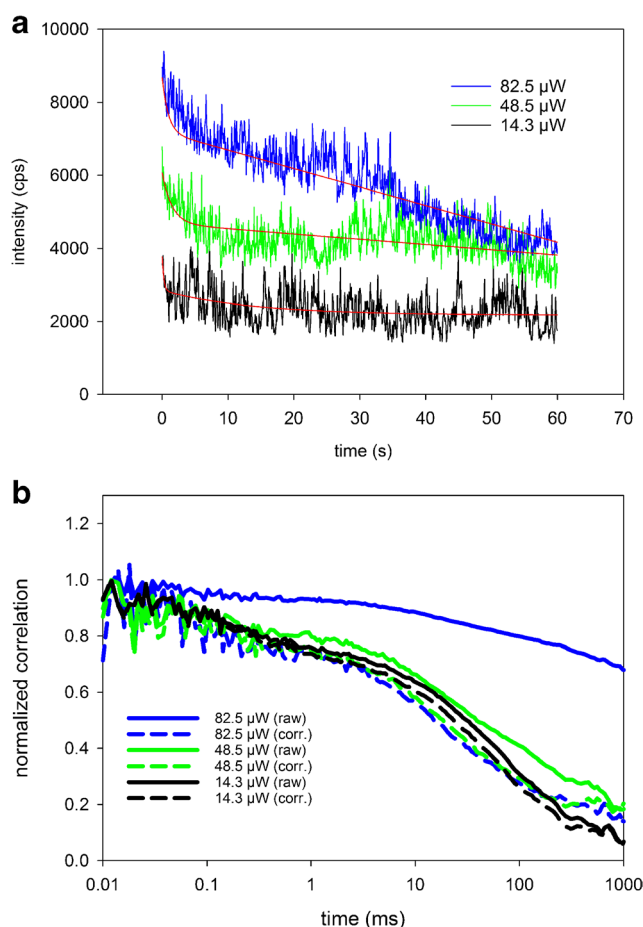


Fig. 4 Correcting experimental data from Cy5 diffusing in glycerol solution for photobleaching. **a** shows the fluorescence intensity as a function of time, together with bi-exponential fits, for various excitation intensities photobleaching, leading to different amounts of photobleaching. **b** shows the time correlation functions that are computed from these photon arrival times with and without the photobleaching correction. After applying the correction algorithm, all curves align

weigh the photons according to their arrival time with the weighting function determined from bi-exponential fits to the intensity, all curves collapse onto a single curve that is very close to the uncorrected autocorrelation function at the lowest intensity, where photobleaching is almost absent.

The quality of the data is sufficient to further reconstruct mean-square displacements from the autocorrelation functions using the analytical expression of Eq. (7). The result is shown in Fig. 5a. We note that we obtain essentially identical mean-square displacement reconstructions for all data sets taken at different intensities, even though the raw, uncorrected correlation functions were rather different. This illustrates how correcting for photobleaching makes even seemingly unusable data suitable for further consistent, quantitative analysis. The mean-square displacement data appears meaningful for times between 1 and 300 ms,

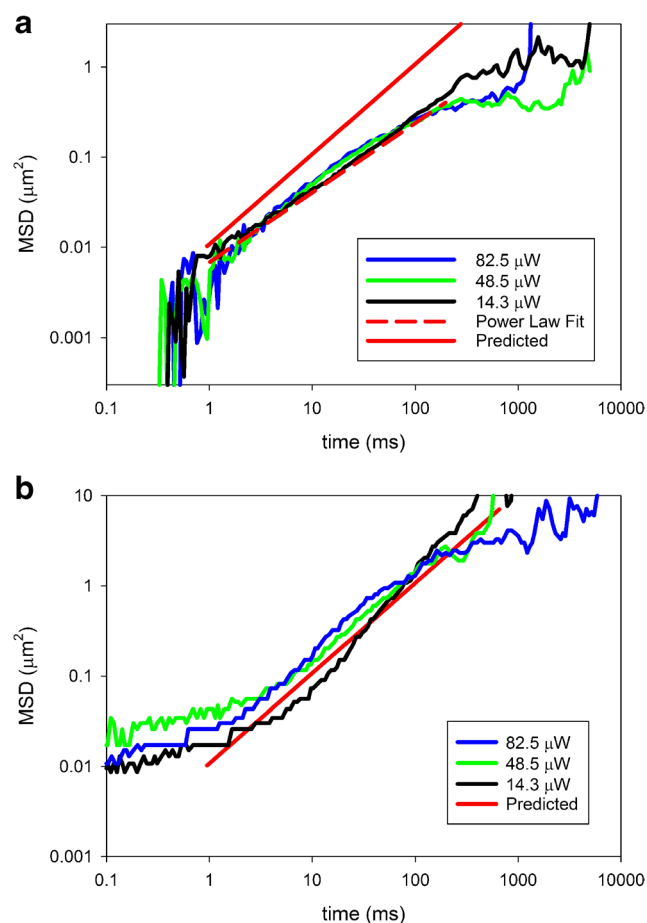


Fig. 5 Mean-square displacement of Cy5 in glycerol solution, as calculated from an inversion of Eq. (7) in (a) and from a lookup table from a calibration run according to Eq. (8) in (b). The solid lines show the mean-square displacements that are recovered from the correlation functions after correction for photobleaching. A fit to a generic power law is indicated by the dashed red line, the red solid line shows the expected mean-square displacement of the dye assuming normal diffusion and a viscosity 200x higher than water

corresponding to a range of absolute displacements between 80 and 250 nm.

From this, we calculate for short time scales around 1 ms a diffusion coefficient of $7 \cdot 10^{-12} \text{ m}^2 \text{ s}^{-1}$, which is indistinguishable from the expected diffusion coefficient that is calculated from the estimated viscosity of the glycerol solution at room temperature and the diffusion coefficient of Cy5 in water. We also find that the motion appears to be somewhat subdiffusive following a power law with an exponent of $\nu = 0.77$. Since this behavior was not observed in our simulations, where the recovered motion was always diffusive, if not slightly super-diffusive, we ascribe it to an experimental artifact, most likely deviations of the actual beam profile from a pure Gaussian.

To account for the larger than expected contributions to the signal from far-out molecules in the case of a non-Gaussian beam, we used directly the calibration correlation functions that were collected with Cy5 in aqueous solution to compute the mean-square displacement according to Eq. (8). The results are shown in Fig. 5b. The mean-square displacements as a function of time are now generally indistinguishable from normal diffusion, although at the expense of some minor distortions and added noise at short time scales.

Conclusions

In conclusion, we have demonstrated that fluorescence correlation spectroscopy can be used quantitatively even in slowly diffusing systems that are subject to considerable photobleaching. Photobleaching-induced artifacts in the correlation functions can be removed numerically during the data analysis process by calculating the correlation functions from the arrival times of the photons, where each photon is assigned a proper weight to compensate for already lost fluorophores. The corrected correlation functions can then be used to calculate the mean-square displacements of the particles. To overcome artifacts from imperfections in the excitation beam at larger time scales, it may be advantageous to use a direct calibration based on a reference correlation function with a known diffusion coefficient instead of the usual analytical process. With these considerations in the data analysis process, quantitative data can be obtained even in challenging samples, opening up new applications in complex fluids and live cells.

Acknowledgements This work was funded through internal resources of the University of Michigan. The experimental portion was carried out at the Single-Molecule Analysis in Real-Time (SMART) Center with equipment acquired through NSF MRI-ID grant DBI-0959823 to Nils G. Walter. Michael S. Jones contributed to the simulations and data analysis. The authors would like to thank Jörg Enderlein from the University of Göttingen for generously sharing computer code for the calculation of correlation functions from photon arrival times with us.

References

- Magde D, Elson E, Webb WW (1972) Thermodynamic fluctuations in a reacting system – measurement by fluorescence correlation spectroscopy. *Phys Rev Lett* 29:705–708. <https://doi.org/10.1103/PhysRevLett.29.705>
- Krichevsky O, Bonnet G (2002) Fluorescence correlation spectroscopy: the technique and its applications. *Reports Prog Phys* 65:251–297. <https://doi.org/10.1088/0034-4885/65/2/203>
- Chiantia S, Ries J, Schwille P (2009) Fluorescence correlation spectroscopy in membrane structure elucidation. *Biochim Biophys Acta* 1788:225–233. <https://doi.org/10.1016/j.bbamem.2008.08.013>
- Krouglova T, Vercaemmen J, Engelborghs Y (2004) Correct diffusion coefficients of proteins in fluorescence correlation spectroscopy. Application to Tubulin Oligomers induced by Mg²⁺ and Paclitaxil. *Biophys J* 87:2635–2646. <https://doi.org/10.1529/biophysj.104.040717>
- Gröner N, Capoulade J, Cremer C, Wachsmuth M (2010) Measuring and imaging diffusion with multiple scan speed image correlation spectroscopy. *Opt Express* 18:21225–21237. <https://doi.org/10.1364/OE.18.021225>
- Du ZX, Dong CQ, Ren JC (2017) A study of the dynamics of PTEN proteins in living cells using in vivo fluorescence correlation spectroscopy. *Meth App Fluoresc* 5:024008. <https://doi.org/10.1088/2050-6120/aa6b07>
- Michelman-Ribeiro A, Mazza D, Rosales T, Stasevich TJ, Boukari H, Rishi V, Vinson C, Knutson JR, McNally JG (2009) Direct measurement of association and disassociation rates of DNA binding in live cells by fluorescence correlation spectroscopy. *Biophys J* 97:337–346. <https://doi.org/10.1016/j.bpj.2009.04.027>
- Dunsig V, Mayer M, Liebsch F, Multhaup G, Chiantia S (2017) Direct evidence of amyloid precursor-like protein 1 trans interactions in cell-cell adhesion platforms investigated via fluorescence fluctuation spectroscopy. *Mol Biol Cell* 28:3609–3620. <https://doi.org/10.1091/mbc.E17-07-0459>
- Widengren J, Thyberg P (2005) FCS cell surface measurements – photophysical limitations and consequences on molecular ensembles with heterogenic mobilities. *Cytometry A* 68A:101–112. <https://doi.org/10.1002/cyto.a.20193>
- Widengren J, Rigler R (1996) Mechanisms of photobleaching investigated by fluorescence correlation spectroscopy. *Bioimaging* 4:149–157. [https://doi.org/10.1002/1361-6374\(199609\)4:3<149::AID-BIO5<3.0.CO;2-D](https://doi.org/10.1002/1361-6374(199609)4:3<149::AID-BIO5<3.0.CO;2-D)
- Wahl M, Gregor I, Patting M, Enderlein J (2003) Fast calculation of fluorescence correlation data with asynchronous time-correlated single photon counting. *Opt Express* 11:3583–3591. <https://doi.org/10.1364/OE.11.003583>
- Weber SC, Spakowitz AJ, Theriot JA (2012) Nonthermal ATP-dependent fluctuations contribute to the in vivo motion of chromosomal loci. *PNAS* 109:7338–7343. <https://doi.org/10.1073/pnas.1119505109>
- Ramadurai S, Holt A, Krasnikov V, van den Bogaart G, Killian JA, Poolman B (2009) Lateral diffusion of membrane proteins. *J Am Chem Soc* 131:12650–12656. <https://doi.org/10.1021/ja902853g>
- Online tool (http://www.met.reading.ac.uk/~sws04cdw/viscosity_calc.html) by C. Westbrook, based on Cheng NS (2008) Formula for the Viscosity of a Glycerol-Water Mixture. *Ind Eng Chem Res* 47:3285–3288. <https://doi.org/10.1021/ie071349z>
- Ito S, Sugiyama T, Toitani N, Katayama G, Miyasaka H (2007) Application of fluorescence correlation spectroscopy to the measurement of local temperature in solutions under optical trapping conditions. *J Phys Chem* 111:2365–2371. <https://doi.org/10.1021/jp0651561>
- Kubečka J, Uhlik F, Košovan P (2016) Mean squared displacement from fluorescence correlation spectroscopy. *Soft Matter* 12:3760–3769. <https://doi.org/10.1039/c6sm00296j>